Numerical simulations for quantitative analysis of electrostatic interaction between atomic force microscopy probe and an embedded electrode within a thin dielectric: meshing optimization, sensitivity to potential distribution and impact of cantilever contribution

Menouar Azib, Fulbert Baudoin, Nicolas Binaud, Christina Villeneuve-Faure, Florian Bugarin, Stéphane Segonds, G. Teyssedre

Numerical simulations for quantitative analysis of electrostatic interaction between atomic force microscopy probe and an embedded electrode within a thin dielectric: meshing optimization, sensitivity to potential distribution and impact of cantilever contribution.

M Azib[1,2], F Baudoin[1], N Binaud[2], C Villeneuve-Faure[1], F Bugarin[2], S Segonds[2] and G Teyssedre[1]

[1] LAPLACE, University of Toulouse, CNRS, INPT, UPS, 118 route de Narbonne, F-31062 Toulouse, France

[2] Paul Sabatier University; ICA (Clement Ader Institute), 3 Rue Caroline Aigle, F-31400 Toulouse, France

E-mail: azib@laplace.univ-tlse.fr

Abstract. Recent experimental results demonstrated that Electrostatic Force Distance Curve (EFDC) can be used for space charge probing in thin dielectric layers. A main advantage of the method is claimed to be its sensitivity to charge localization, which, however, needs to be substantiated by numerical simulations. In this paper, we have developed a model which permits to compute EFDC accurately by using the most sophisticated and accurate geometry for the Atomic Force Microscopy (AFM) probe. To avoid simplifications and in order to reproduce experimental conditions, EFDC has been simulated for a system constituted of a polarized electrode embedded in a thin dielectric layer (SiNx). The individual contributions of forces on the tip and on the cantilever have been analysed separately to account for possible artefacts. The EFDC sensitivity to potential distribution is studied through change in electrodes shape, namely the width and the depth. Finally, the numerical results have been compared with experimental data.

PACS number: 02.30.Jr, 07.79.Lh, 68.37.Ps, 73.61.-r, 47.61.Fg

MSC number: 35J05, 93A30, 74B05, 78M10

1. Introduction

A fundamental property of all solid dielectric materials is their ability to accumulate electrical charges under electric stress beyond an electric field threshold. The accumulation of electrical charges induces a local increase of the electric field which can lead to systems failure and/or a premature dielectric breakdown [1, 2]. As example, the excess charges present in thin dielectric layers used in Radio-Frequency Microelectromechanical System (RF-MEMS) [3] is the principal cause of failure of switches with electrostatic actuation. Indeed, the values of applied voltage between the switching actuator and the substrate, needed for actuation, are modified due to electrical charges trapping in the dielectric layer. Hence, after a certain number of events the switch remains in down position due to electrostatic force. Consequently, the development of diagnostic means with a high spatial resolution to localize the accumulated charges corresponding to the real conditions of materials, such as their geometry, is needed to improve the reliability of devices and systems. Up to now, several methods for charge detection in insulators have been proposed to probe charges spatial distribution across the materials such as methods based on acoustic [4] or thermal [5] perturbations. The charge density profile provided by these methods with in-depth resolution is around 1 micrometer to the best and often without lateral resolution. Indeed, the in-depth information given by these methods is not sufficient to investigate accurately thin dielectric films (with a thickness of less than 1μm) and interface phenomena.

Atomic Force Microscopy (AFM) [6] has been known as a useful instrument for nanometer-scale materials diagnostics [7, 8] and for investigating the electrical properties of metallic or insulating materials. Concerning charges detection in thin dielectric layers, techniques derived from AFM such as Kelvin Probe Force Microscopy (KPFM) [9–11] and Electrostatic Force Microscopy (EFM) [12–14] are used. However, these techniques fail to determine the vertical localization of charges [15]. To overcome this issue, a new technique named Electrostatic Force Distance Curve (EFDC) has been proposed [16]. The EFDC is based on the measurement of the electrostatic force between the AFM probe and the sample using Force Distance Curve (FDC) measurement [17]. Some experimental results show that EFDC seems sensitive to potential [18] and charges localization in 3 dimensions [16, 19]. However, precise electrostatic models supporting the idea are still lacking. Models based on analytical modelling of AFM tip components [20–22], equivalent charge method [23,24] or Finite Element Method (FEM) [24-26] were developed for quantifying the interactions of the AFM tip with a charged surface or volume. The analytical model failed to predict the electrostatic force over entire distance range (i.e. from 1 nm to 1μm). R. Arinero *et al*. [24] demonstrated that the equivalent charge method and FEM provide best results compared to the analytical model. One of the limits of all of these models is to approximate the AFM tip by 2D-axisymetric truncated cone which does not reproduce the real tip shape and most of the time without any cantilever modelling. A sophisticated model with an accurate geometry of the tip and the cantilever was developed in [25] in which a three dimensional electrostatic model to estimate the electrostatic force between the AFM probe and a

dielectric layer free from charges was developed. Hence, various geometries of the AFM tip were tested: cone, pyramid and tetrahedron. These simulations enabled to establish which geometry of the AFM tip should be considered, showing that an accurate matching between experiment and simulated electrostatic force curves can be obtained using real tip geometry.

After all, the final goal of this research project is to evaluate the ability of EFDC to localize in 3D the charges stored into a thin dielectric using an inverse modelling. Given an experimental EFDC map the aim of the inverse model will be to find a 3D localization of corresponding charges, using this localization as input for the forward model. The forward finite element model allows us to simulate the electrostatic force curves for those charges. One could say that the inverse model treats EFDC as an input variable, and the charges localization as an output variable. The use of the inverse model is quite a cumbersome computational task. Therefore one has to look for possible ways to improve the performance. There is therefore a need for reducing the computational time of the forward model; as the inverse model will perform a big number of evaluations of the cost function in order to get the best solution. To shorten the computation time of the forward model, the mesh has to be optimized. This is not a straightforward task because the studied geometry presents a big scale disparity between its components; for example the apex radius is of the order of 25nm when the height of the tip is 10µm. As a result, the finite element meshing generates too many elements in order to build a complete mesh of this geometry. In this case the simulation takes a too long computation time to get solved.

It should be pointed out that the study developed in [25] is considered as a first step for evaluating the capability of EFDC to localize charges in thin dielectrics as it gives a convenient geometry of the AFM probe. However, in this study, the tilt angle of the tip and the cantilever are not taken into account. At that time, it seems that no study has been reported about the influence of mesh construction on the performance of the forward model, which is the important element of the inverse modelling. This is the reason why the next step of this research project is to propose a numerical model with a suitable and optimized mesh for the geometry given in [25]. The efficiency of model resolution has to be improved, the computational time reduced, so as to simulate the electrostatic interactions between a conductive AFM probe and buried electrodes embedded in a thin dielectric material. The choice of modelling EFDC with buried electrodes instead of a charges cloud is directly supported by the fact that this could be tested experimentally with the AFM. Hence, the results of this model can be compared with the experimental ones and the influence of the lateral and vertical potential distribution on EFDC investigated.

The traditional way of probing electrostatic phenomena at dielectric surface is with charging with the AFM tip and then scanning with the AFM probe. The method brings unknown on the actual field at play during charging owing to the strongly divergent nature of the field produced by the tip: as a consequence the charging mechanism cannot be accurately investigated in terms of field dependence. In order to bring more control of the field during charging, the EFDC measurements are realized along the crossed direction between buried electrodes. The electrodes can be biased for charging [27]. The

use of an embedded electrode constitutes a good model for simulation as the hypothesis on the source of force, i.e. the potential applied to the electrode is perfectly known. In the following, electrostatic modelling is achieved for this configuration of a single buried electrode. The influence of the width and depth of the electrode on the EFDC is investigated using experimental results and simulation to validate our approach.

The paper is structured as follows. In section 2, samples and EFDC measurement are described. The sections 3 and 4 are devoted to simulate tip and cantilever respective contributions to electrostatic force. Finally, the paper is closed by a summarizing conclusion and inferences.

2. Experimental conditions

Samples are composed by aluminium electrodes embedded in SiNx dielectric layer elaborated by Plasma Enhanced Chemical Vapour Deposition (PECVD) over silicon substrate. Different parameters as electrode width W and distance d between electrode and sample surface are used. Details about sample processing are reported elsewhere [19]. EFDC measurements were performed on the Bruker multimode 8 setup using Pt-coated silicon tip, model SCM-PIC-V2 from Bruker. Measurements were done under nitrogen atmosphere after sample drying at 100°C during 15min to remove water film. The spring constant of the cantilever was estimated to 0.36Nm^{-1} using thermal tune mode.

3. Electrostatic tip model

Numerical simulations of EFDC were conducted using a commercial finite element solver: COMSOL Multiphysics® with the AC-DC module [28]. At first, we built a geometry that matches accurately the actual configuration used in the AFM experimental setup as presented in section 2, including the shape of the tip and the electrode embedded in the dielectric layer as represented on figure 1. From an electrostatic point of view, the fact that the tip is coated with platinum produces a isopotential situation at the surface of tip. Therefore the tip is modelled as a homogeneous medium.

3.1 Geometry description

Our general approach was to calculate the electrostatic force interaction on stationary tip as a function of its position over the infinite dielectric layer (SiNx) of thickness e of 270nm and a relative permittivity of 7.5. The electrode within this dielectric layer is described as a finite aluminium layer with a thickness e of 70nm; a depth d and a width W (see figure 1a). The tip is modelled by the most relevant shape [25] (see figure 1c): a spherical-tetrahedral shape with tip apex of radius R = 25nm (see figure 1b), tip tetrahedron half-angle of 20°, tip height L = 10µm and tilt angle α = 16°, in order to match the characteristics of experimental probes (see figure 1c). To simulate the EFDC, the electrostatic force **F** is computed for different distances between the tip and the dielectric surface, denoted D, with a range from 0 to 200nm. The tip is supposed to be surrounded by an air box whose dimensions are large enough to avoid edge effects. The cantilever itself is not represented here, because its contribution will be investigated in section 4. Indeed a 3D electromechanical model is

presented in section 4 to evaluate the contribution of the second part of the AFM probe, the cantilever, in the EFDC. So, in this section the study is reduced to the calculation of the force exerted on the tip as a function of tip-dielectric separating distance using the electrostatic model.

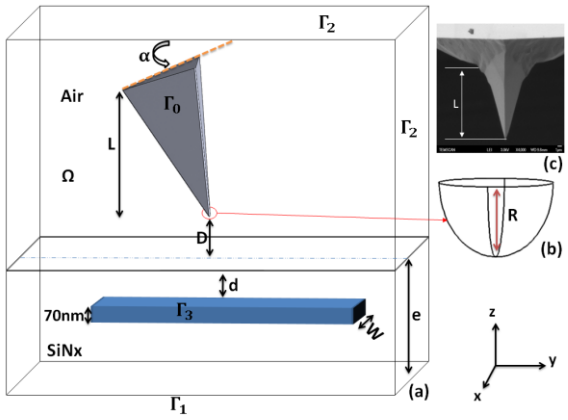

Figure 1. (a) Description of the geometry used for tip- modelling. (b) A zoom of tip apex, (c) Scanning electron microscope image of the tip.

3.2 Equations

In the present electrostatic model, the first step is to determine the potential distribution in air box and dielectric layer. The following step is to estimate the electrostatic force induced on the tip by the applied voltage to the electrode. This determination requires the resolution of the Poisson's equation (eq. 1) in the domain Ω, with taking into account the boundary conditions on the interface Γ (see figure 1). Γ is composed of three parts Γ_0, Γ_1, Γ_2 and Γ_3. The problem is written as follows:

$$\mathrm{div}(-\varepsilon\,\mathbf{grad}(V)) = 0 \ \text{ in } \Omega \qquad (1)$$

$$V = 0 \text{ on } \Gamma_0 \text{ and } \Gamma_1 \qquad (2)$$

$$V = V_0 \text{ on } \Gamma_3 \qquad (3)$$

$$\frac{dV}{d\mathbf{n}} = 0 \text{ on } \Gamma_2 \qquad (4)$$

Where V_0 is the applied voltage (constant) on the electrode **n** is the vector normal to the surface and ε is the permittivity of the dielectric or the air. The tip surface (Γ_0) and the back side of the dielectric (Γ_1) are set to the ground.

3.3 Electrostatic Force Distance Curve (EFDC)

The electrostatic force **F** acting on the tip surface was computed by the integration of the built-in Maxwell-stress-tensor, Mt, over all faces of the tip:

$$\mathrm{Mt} = \frac{\varepsilon_0}{2}\|\mathbf{E}\|^2 \qquad (5)$$

$$\mathbf{F} = \int_{\Gamma_0} \mathrm{Mt}.\mathbf{n}.\mathrm{ds} \qquad (6)$$

With **E** is the electric field, being the gradient of the potential V. To simulate the electrostatic force distance curve, the electrostatic force **F** is computed for an applied potential $V_0 = 15V$ on the surface of the electrode and for different tip-sample distances from 0nm to 200nm, in step of 4nm.

3.4 Mesh optimization for EFDC computing

In order to solve numerically the Poisson's equation in the domain Ω and to determine the electrostatic force, the FEM has been applied for discretizing the geometry. For the FEM, meshing is the primordial stage, because the numerical error is directly linked to its quality. One of the key points about meshing quality was the idea of mesh convergence; as the mesh is refined, the solution will be more accurate. Besides, when it comes to setting up and solving a finite element problem, meshing is one of the most memory-intensive steps. Our geometry presents a huge scale disparity between its components, for example, between the tip height (≈ 10µm) and the apex radius (≈ 25nm), the dielectric thickness (≈ 270nm) and the electrodes (dimension from few microns to tens of microns). This disparity will lead to generate too many elements by the mesh if a standard meshing is applied. If the mesh is using too many elements the simulation will take a large amount of computational time to solve. Modelling geometries with high scale disparity is one of the most difficult tasks for the finite element analyst.

In such case it is advisable to switch to user-controlled mesh to manually build and edit the meshing sequences available in the COMSOL Multiphysics software as an alternative to using the default meshing sequence. In that aim, the regions where the electrostatic interactions are very high need to be meshed finely and the ones representing weak interactions need to be meshed coarsely. According to relations (5) and (6), the electric field is the crucial parameter governing the electrostatic interaction force in the near-field microscopy and is very sensitive to the AFM tip curvature radius [28]. In words, these relations mean that the strength of the electric field at any point in space is the rate of change of the electrostatic interaction force over space. If the electrostatic force changes significantly over a small distance (as in the region near the tip apex), the electric field is strong; if the electrostatic force changes only by a small amount over a large distance (as in the region far away from the tip apex), then the electric field is weak. Therefore, we need to plot out the electric field distribution **E** to spot the zones where the electrostatic interactions are higher. Two mesh strategies were used to evaluate our optimization process.

The default meshing was done using the default "Physics-Controlled Mesh capability", which is automatically created. This mesh is a simple, unstructured tetrahedral mesh and with the element size defaulting to extremely fine (2×10^{-9} m for the minimal element size to 2×10^{-7} m for the maximum element size with element growth rate set to 1.3) in order to have accurate reference electric field distribution. If one goes ahead and mesh this geometry with just the default Physics-Controlled Mesh

capability with element size set to extremely fine, a mesh will be obtained like that pictured below (see figure 2).

The resulting mesh of our geometry consists of about 3,520,449 elements, the computation time needed to solve Poisson's equation with this mesh for D = 0nm, d = 100nm, W = 6µm and V_0 = 15V is about 300s. For the entire curve (40 points) it requires more than 16h.

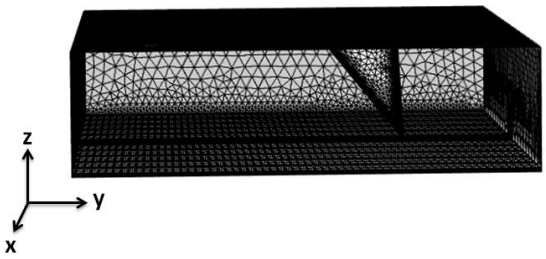

Figure 2. An unstructured tetrahedral mesh with the element size set to extremely fine on the tip-dielectric component geometry. D = 0nm, d = 100nm, W = 6µm and V_0 = 15V.

The following step is to plot out the magnitude of the electric field distribution recorded over the tip surface, so as to determine the regions where **E** is high or weak. Figure 3 shows that the maximum norm of the electric field Emax is reached on the tip apex, which confirms that the electrostatic force is dominated by the contributions from the tip apex.

In order to select the regions where the electric field is strong, we have defined a threshold, which is here about 10% of Emax. Thus, it is considered that in regions where the electric field values are above this threshold, electrostatic interactions are strong (the region delimited by a red dashed line in figures 3a and 3b); otherwise the interactions are weak. Then, the region where the electric field is strong can be represented by a cylinder in the simplest form, which has a radius equal to a/2 (figure 3a) and a height equal to C (figure 3b).

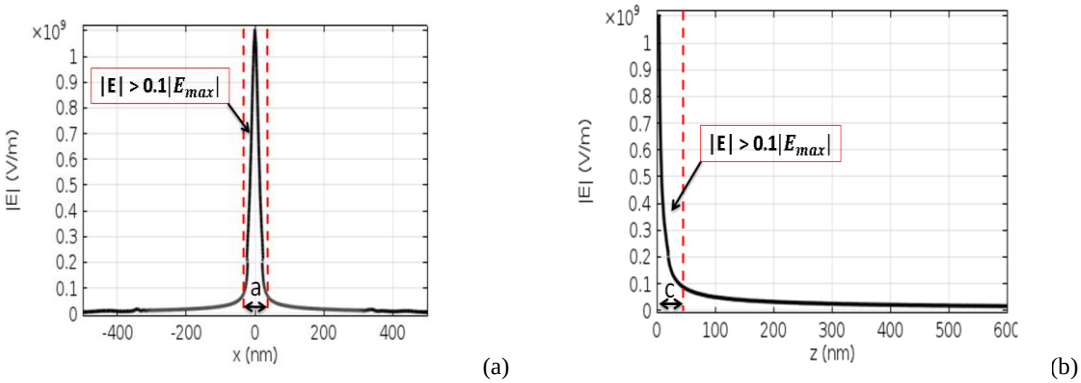

(a) (b)

Figure 3. The electric field recorded (a) over the surface of the tip along the x-axis and (b) vertically between tip and sample surface along z-axis. D = 0nm, d = 100nm, W = 6µm and V_0 = 15 V.

The optimized meshing uses these considerations. This cylinder, surrounding tip apex, is added to our geometry without any boundary conditions, and is meshed very finely whereas the rest of the

geometry is meshed coarsely (see figure 4). However, for the electrode and the dielectric a swept meshing is used to deal with thin objects (electrode thickness = 70nm and dielectric thickness = 270nm). The idea behind using swept meshing is to have a mesh that represents accurately the geometry and provides reliable solution, without many elements, as solving our models would then require excessive computational resources. In addition, we know that the electrostatic interactions between tip and dielectric are mostly vertical; for this reason we need to mesh more finely in vertical direction.

A 2D quadrilateral surface mesh was used at the bottom face of the dielectric with element size set to extremely fine, and then it was swept along the entire length of the dielectric to create quadrilateral prismatic elements. Finally, quadrilateral faces created were converted into triangular faces because of adjacent face constraint: this is at the horizontal contact face between the block of air and the dielectric, where we have meshed everything using free tetrahedral operations with element size set to coarse (1.9×10^{-6} m for the minimal element size to 2.6×10^{-5} m for the maximum element size with element growth rate set to 1.4).

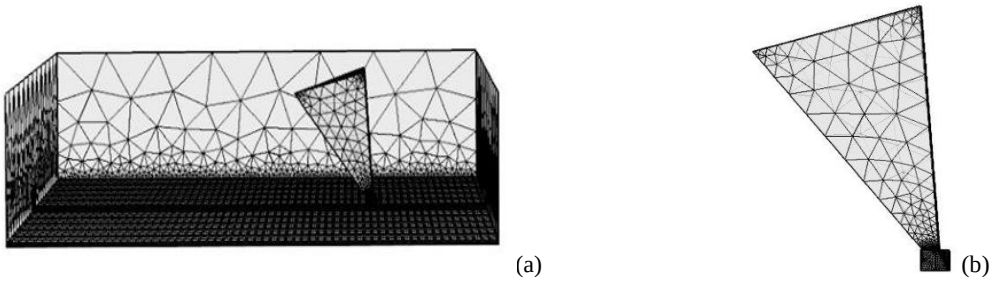

(a) (b)

Figure 4. The structured and optimized mesh over the entire geometry (a): the space around the apex (b) was meshed finely as the default one, the dielectric and the electrode were meshed by using the swept mesh advanced option and the remaining space was meshed coarsely.

Table 1 compares the number of elements and computing time for each meshing method. The time spent to simulate the entire curve when using optimized meshing is 30 times less than the one with default meshing, while the disparity between the two curves is in the order of $10^{-4.}$ It can be concluded that taking in consideration the disparity of the modelled objects scale and the three-dimensionality of the system, the error is acceptable. Therefore, the computational time of the model has been reduced without affecting the quality of the result, which is the main objective of this work. However, this section addresses only the tip mesh optimization without introducing the cantilever model yet.

Table 1. Optimization results

Mesh	Elements	Time(s)	Disparity between two curves
Automatic	3,520,449	60 000	10^{-4}
Optimized	683,504	2 000	

3.5 Comparison with experimental curves

In the following, the numerical results obtained by the electrostatic model for the tip and the experimental are compared. EFDCs were measured and computed for an applied potential electrode V_0 =15V, for different electrode width W and different electrode depth d from the dielectric surface. Figure 5 represents the evolution of the electrostatic force as a function of the vertical distance separating the tip and the sample surface: (a) for different electrode width and (b) for different electrode depth. In the model as well as in the measurement, the AFM tip is placed above the middle of the embedded electrode. Generally, these force curves decrease steeply for very small tip-sample distances and then exhibit a curvature to finally approach some horizontal asymptote. This shape is verified both in experiment and modelling. Changing the width of the electrode does not lead to substantial change in the electrostatic force at short distance. This is presumably because the tip width is much smaller than the width of the electrode. As distance increases, the force is all the larger that the electrode is wider, which can be understood by an increasing contribution from electrode edges. This is verified both in measurement and modelling. The impact of electrode depth is different. First, both measurement and model show that the interaction force at short distance is much larger for the shorter depth. Second, an asymptotic limit is reached both in measurement and modelling, but the level is the same in case of the model and different in the experiments.

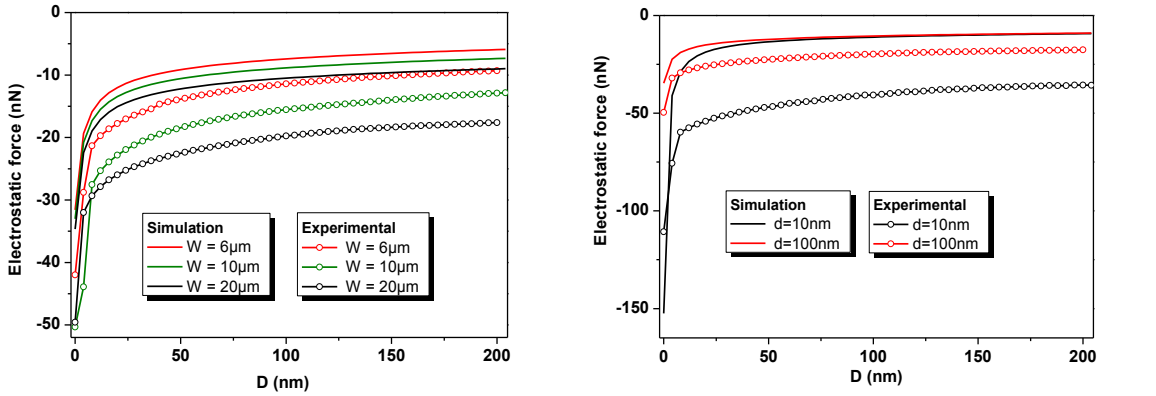

(a) (b)

Figure 5. Comparison between simulated (tip only) and experimental EFDC: (a) for different electrode width W (6µm, 10µm and 20µm), and an embedded distance d = 100nm, (b) for different electrodes depth d with the electrode width set to 20µm. 15V was applied on the electrode.

It should be noted that, the parameters W and d are linked respectively to the lateral potential distribution and the vertical potential distribution. Thus, the EFDC is sensitive to lateral and vertical

potential distribution through the tip contribution. At first glance, computed and experimental EFDC exhibit similar shape but present an offset by about some tens of nN for each configuration. This offset is presumably linked to the contribution to force due to the cantilever [25] which is not taken into account here. To quantify accurately this contribution, an electromechanical model is presented in the following. The cantilever was modelled as a semi-clamped beam without the tip. According to superposition principle, the contribution from cantilever to the force will be added to the one from the tip in order to compare experimental EFDC to simulated one.

4. Cantilever electromechanical model

4.1 Geometry description

The cantilever is modelled as a semi-clamped beam with a smooth rounded corner to avoid edge effects. It is placed at a distance L+D from the dielectric surface, L and D being respectively the total height of the tip and the separating distance between the tip and the sample.

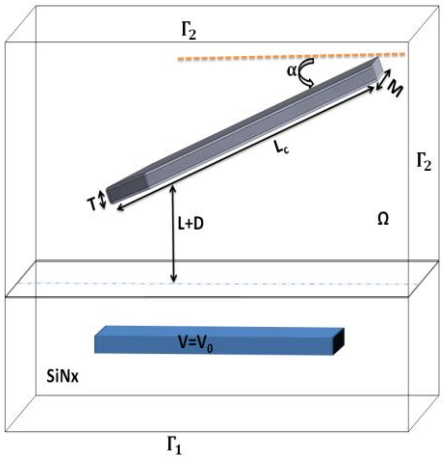

Figure 6. Sketch of the geometry of cantilever beam-dielectric system used in electromechanical model.

The elastic cantilever beam is fixed at the right end (mechanical fixed constraint) and tilted by the same angle as the axis of tip, i.e. $\alpha = 16°$ (see figure 6). The electromechanical study combines electrical and mechanical processes, so it requires substantially more memory and computational resources to compute the distribution of the electric field than in the electrostatic model used for the tip.

Several geometric parameters characterizing the cantilever beam geometry are shown in table 2: the thickness T, the width M, the length L_c and the spring constant k which are related by the expression:

$$k = \frac{E.M.T^3}{4.{L_c}^3} \qquad (7)$$

Where E is the Young's modulus.

Table 2. Geometric parameters of the cantilever beam

Material	Spring constant k(Nm^{-1})	Thickness T(µm)	Width M(µm)	Length Lc(µm)	Young's modulus E(GPa)
Si/PtIr	0.36	2.5	55	450	165

4.2 Equations and results

The primary problem the electromechanical model addresses is the 2-way coupling between the deformation (mechanical domain) and the electric field (electrical domain). The model solves the deformation of the beam due to the electrostatic force induced by an applied potential difference between the cantilever and the embedded electrode. As the beam bends towards sample surface, the geometry of the air-filled space changes continuously. The model takes this displacement into account when computing the potential field. Thus, the geometry deforms, and the electric field between the cantilever and the electrode continuously changes as a result of the bending. That is why two equations need to be solved:

i/ the Poisson's equation (1) in the surrounding air Ω of boundaries Γ_1 and Γ_2. Here, a constant potential V_0 is applied at the surface of the electrode, the surface of the cantilever and the bottom of the dielectric (Γ_1) are set to ground.

ii/ the mechanical equation which provides the displacement of the beam in the stationary case:

$$\nabla . \boldsymbol{\sigma} = \mathbf{F_v} \qquad (8)$$

Where $\boldsymbol{\sigma}$ is the stress tensor and $\mathbf{F_v}$ is the force exerted on the volume. The stress tensor must be continuous between the air and the cantilever.

$$\mathbf{n}(\boldsymbol{\sigma}_{\text{air}} - \boldsymbol{\sigma}_{\text{beam}}) = 0 \qquad (9)$$

where $\mathbf{n}$ is the outward normal vector of the domain surrounding the cantilever.

In order to solve numerically this electromechanical problem the type of mesh needs to be defined. We used the same meshing as for the electrostatic tip model. For the cantilever we used also a swept mesh with the element size set to normal in order to reduce the degree of freedom (see figure 7). After setting up the meshing process, the displacement at the end of the cantilever beam Δz is computed and then the electrostatic force **F** exerted on the cantilever is calculated by the Hook's law:

$$\|\mathbf{F}\| = \mathrm{k}.\Delta \mathrm{z} \qquad (10)$$

Despite the fact that a structured and swept mesh was used, a huge computational time is necessary in order to get the displacement of the beam and plot out the EFDC. We attribute this cost to the fact that

our 3D geometry presents a huge scale disparity between its components such as the thickness of the electrode =70nm and the length of the cantilever =450µm. In addition, as stated previously, the electromechanical study couples two physics: electrostatics and solid mechanics. So, during the discretization process the finite element software generates a huge number of degrees of freedom (DOF), which is a crucial memory requirement. To face this problem and cut down on the time required to run the simulation, we have used a powerful machine with 32 GB RAM.

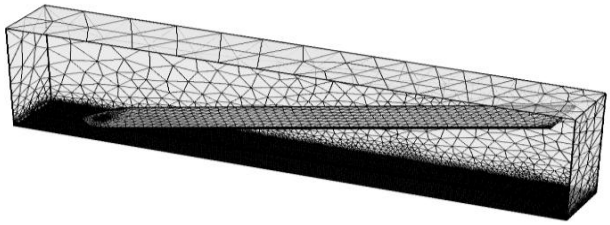

Figure 7. A structured and optimized mesh over the entire cantilever-dielectric system: the cantilever was meshed using a swept mesh with element size set to normal.

The calculus that COMSOL Multiphysics needs to store fits entirely within RAM. If the allocated memory is not enough, part of the calculus will spill over to the hard disk. Thus, the performances of all programs running on the computer are degraded. If excessive memory space is requested by the COMSOL software, then the operating system will determine that it cannot anymore manage memory efficiently (even via the hard disk) and will tell that there is no more memory space available for the application. When this occurs, an "out-of-memory" warning appears and COMSOL Multiphysics stops solving the model. After all, our simulation required 10 hours in order to obtain the cantilever contribution over the tip-sample distance range (40 points from 0nm to 200nm by step of 4nm) and 30GB hard disk space was used.

The total electrostatic force between a typical embedded electrode and the AFM probe obtained by modelling and the experimental data are plotted in figure 8. The individual contributions from the lever and the tip tetrahedron are also shown.

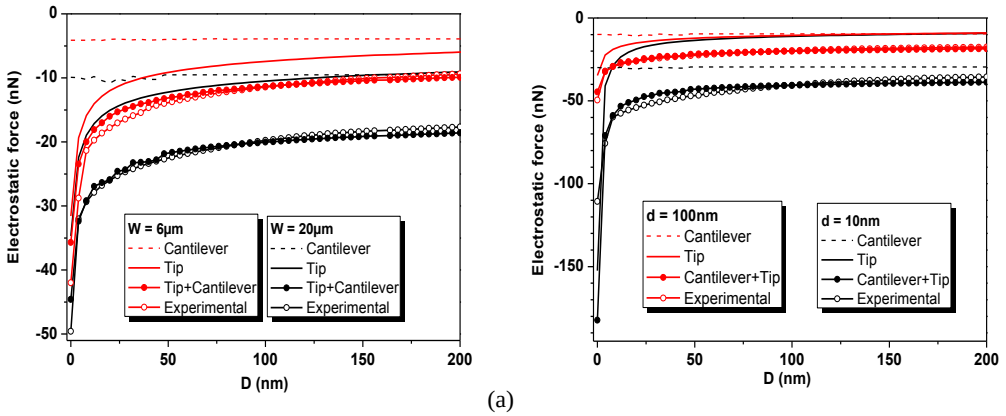

Figure 8. Comparison between simulated (tip + cantilever) and experimental EFDC (a) for various electrode width with a fixed electrode depth set to 100nm and (b) for various electrode depth with width set to 6µm. The

cantilever contributions are plotted using dashed lines. For simulation and experiments, the applied potential V_0 was fixed at 15V.

As it can be seen from the figures and as expected, the contribution of cantilever beam is a nearly constant component with the tip-dielectric distance for each configuration. The lever contribution respectively for W = 6µm and W = 20µm is -4nN and -10nN. In addition, the variation of the depth d (d = 100nm, d = 10nm) modifies the lever contributions from -10nN to -30nN. These results show that not only the tip, and also the cantilever is sensitive to the lateral potential distribution (through W) and to the vertical potential distribution (through d). Even though this cantilever is far from the sample, approximately about 10µm, it contributes very strongly to the total force due to the long-range character of electrostatic interaction and also to the large size of the electrode. Thus, the lever contribution cannot be neglected when interpreting EFDC measurements.

The superposition principle is applied for summing up the microscopic tip contribution with the macroscopic cantilever contribution to obtain the total force exerted on the entire AFM probe.

Figure 8 reveals a very good agreement between the experimental EFDC and the simulated ones (tip + cantilever). Small differences between experimental and simulated EFDC for short distance range can be due to differences between tip apex radius used in simulation and the real shape.

Although the cantilever contribution is sensitive to the width and depth of the embedded electrode, it is noticeable from Figure 8 that the electrostatic force is weakly varying with the distance. Hence at this step, a linearization of the contribution of the cantilever to the force vs. D is possible. For given depth and width, the force will be computed at only two points for example at the contact (D = 0nm) and at long distance (D=200nm), linearized, and will be added to the contribution due to tip. Thus, we reduce time from 10 h to 24 minutes for the electromechanical model. However, this time is still long for the inverse model using EFDC to localize charges in thin dielectric.

5. Conclusion and perspectives

A realistic and complete model for electrostatic interaction between AFM probe and a flat thin dielectric layer (SiNx) has been developed. In order to reproduce experimental conditions and to base the work on well controlled source of force, EFDC were simulated over a polarized buried electrode within the dielectric. Results reveal a very good agreement between model and experimental data. The model takes into account the contributions from the macroscopic cantilever by means of an electromechanical model, the micrometric scale tip and the nanometre scale apex by means of an electrostatic model. Results provided by the model emphasize that the EFDC is sensitive to the lateral and vertical potential distribution through the tip and the cantilever contributions. We found that the cantilever contribution is very important and it cannot be neglected. This certainly has important consequences for interpreting EFDC measurements. It should be noted that the electromechanical

approach which was used to compute the cantilever contribution is demanding both for memory resources and computational time, even using a sophisticated and an optimized mesh.

The final objective of the work is to bring the EFDC to a method for localizing in 3D the charge distribution in a thin dielectric by AFM. The approach requires an inverse modelling for retrieving charge distribution from force map. As a first step, reducing the computational time of the COMSOL model is necessary, as the inverse modelling performs a huge evaluation of the forward model, in order to get the best solution. The only way to go ahead is to simplify the computing of the cantilever contribution. This can be done in two ways, depending on the charge configuration: either charges are very localized and this contribution can be neglected, or the charge is broadly distributed and a linearization is achieved. The analysis of the contribution of the cantilever in presence of injected charges, with nominal charge spot sizes ranging from 10nm to 1µm will shed light on this point. The form and the size of the charge pattern are based on available experiments. We believe that for such sizes of charge cloud the cantilever will not contribute substantially to the total force.

References

[1] Gerhard-Mulhaupt R and Joseph M C 1999 *Electrets* 3rd edn (California: Laplacian)

[2] Normand P et al 2003 Effects of annealing conditions on charge storage of Si nanocrystal memory devices obtained by low-energy ion beam synthesis *Microelectron.* Eng. **6**7 629–34

[3] Wu Y and Shannon M A 2004 Theoretical analysis of the effect of static charges in silicon-based dielectric thin films on micro- to nanoscale electrostatic actuation *J. Micromech. Microeng*. **14** 989–998

[4] Maeno T and Fukunaga K 1996 High-resolution PEA charge distribution measurement system *IEEE Trans. Dielectr. Electr. Insul.* **3** 754–757

[5] Lang S B 1991 Laser intensity modulation method (LIMM): Experimental techniques, theory and solution of the integral equation *Ferroelectrics* **118** 343–361

[6] Binnig G, Quate C F, and Gerber Ch 1986 Atomic Force Microscope *Phys. Rev. Lett.* **56** 930–934

[7] Leach R K et al 2011 The European nanometrology landscape *Nanotechnology* **22** 062001

[8] Hansen H N, Carneiro K, Haitjema H and De Chiffre L 2006 Dimensional micro and nano metrology *CIRP Ann. Manuf. Technol.* **55** 721–743

[9] Rezende C A, Gouveira R F, da Silva M A and Galembeck F 2009 Detection of charge distribution in insulator surfaces *J. Phys.: Condens. Matter* **21** 263002

[10] Ishii M 2010 Static states and dynamic behaviour of charges: observation and control by scanning probe microscopy *J. Phys.: Condens. Matter* **22** 173001

[11] Stevens G C and Baird P J 2005 Nano- and Meso- measurement methods in the study of dielectrics *IEEE Trans. Dielectr. Electr. Insul.* **12** 979

[12] Lambert J, Guthmann C and Saint Jean M 2003 Relationship between charge distribution and its image by electrostatic force microscopy *J. Appl. Phys*. **93** 5369

[13] Gómez-Moñivas S, Froufe-Pérez L S, Caamaño A J and Sáenz J J 2001 Electrostatic forces between sharp tip and metallic and dielectric surface *Appl. Phys. Lett.* **79** 4048–4050

[14] El Khouri D, Arinero R, Laurentie J C and Castellon J 2016 Nanoscale surface charge detection in epoxy resin materials using electrostatic force microscopy *AIP Advances* **6** 035318

[15] Palleau E, Ressier L, Borowik L and Mélin T 2010 Numerical simulations for quantitative analysis of AFM electrostatic nanopatterning on PMMA by Kelvin force microscopy *Nanotechnology* **21** 225706

[16] Villeneuve-Faure C, Boudou L, Makasheva K and Teyssedre G 2014 Towards 3D charge localization by a method derived from atomic force microscopy: the electrostatic force distance curve *J. Phys. D: Appl. Phys.* **47** 455302

[17] Cappella B and Dietler D 1999 Force-distance curves by atomic force microscopy *Surf. Sci. Rep.* **34** 1–104

[18] Alhossen I, Villeneuve-Faure C, Baudoin F, Bugarin F and Segonds S 2017 Sensitivity analysis of the electrostatic force distance curve using Sobol's method and design of experiments *J. Phys. D: Appl. Phys.* **50** 035304

[19] Villeneuve-Faure C, Boudou L, Makasheva K and Teyssedre G 2016 Atomic Force Microscopy Developments for Probing Space Charge at Sub-micrometer Scale in Thin Dielectric Films *IEEE Trans. Dielectr. Electr. Insul.* **23** 705

[20] Hudlet S, Saint Jean M, Guthmann J and Berger J 1998 Evaluation of the capacitive force between an atomic force microscopy tip and a metallic surface *Eur. J.* **2** 5

[21] Marchi F, Dianoux R, Smilde H J H, Mur P, Comin F and Chevrier J 2008 Characterization of trapped electric charge carriers behaviour at nanometer scale by electrostatic force microscopy *J. Electrost.* **66** 538

[22] Colchero J, Gil A and Baro A M 2001 Resolution enhancement and improved data interpretation in electrostatic force microscopy *Phys. Rev.* **64** 245403

[23] Watanabe S, Hane H, Ohye, Ito M, and Goto T 1993 Electrostatic force microscope imaging analyzed by the surface charge method *J. Vac. Sci. Technol.* **11** 1774–1781

[24] Arinero R, Riedel C and Guasch C 2012 Numerical simulation of electrostatic interaction between an atomic force microscopy tip and a dielectric sample in presence of burried nanoparticule *J. Appl. Phys.* **112** 114323

[25] Boularas A, Baudoin F, Teyssedre G, Villeneuve-Faure C and Clain S 2016 3D modelling of electrostatic interaction between AFM probe and dielectric surface: Impact of tip shape and cantilever contribution *IEEE Trans. Dielectr. Electr. Insul.* **23** 713

[26] El Khoury D, Fedorenko V, Castellon J, Bechelany M, Laurentie J-C, Balme S, Fréchette M, Ramonda M and Arinero R 2017 Characterization of Dielectric Nanocomposites with Electrostatic Force Microscopy *Scanning* **2017**, 4198519

[27] Mortreuil F, Villeneuve-Faure C, Boudou L, Makasheva K and Teyssedre G 2017 Charges injection phenomena at metal/dielectric interface investigated by Kelvin Probe Force Microscopy *J. Phys. D : Appl. Phys* **50** 175302

[28] COMSOL Multiphysics 5.1.1.145 2014

[29] Boularas A, Baudoin F, Teyssedre G, Villeneuve-Faure C and Clain S 2013 Multi-dimentional modelling of electrostatic force between atomic force microscopy tip and dielectric surface *Proc. IEEE Int'l. Conf. Solid Dielectr. (ICSD)* 1040–1043